*Article*

# Synthesis, Characterization and Evaluation of the Antibiofouling Potential of Some Metal and Metal Oxide Nanoparticles

**Lucía Blanco-Covián [1], José Ramón Campello-García [1], María Carmen Blanco-López [2],* and Manuel Miranda-Martínez [1],***

[1]   IDONIAL Technology Center—Parque Tecnológico de Asturias, 33428 Llanera, Spain;
      Lucia.Blanco@idonial.com (L.B.-C.); joseramon.campello@idonial.com (J.R.C.-G.)
[2]   Deptartment of Physical and Analytical Chemistry, Institute of Biotechnology of Asturias,
      University of Oviedo, Julián Clavería, 8, 33006 Oviedo, Spain
*   Correspondence: cblanco@uniovi.es (M.C.B.-L.); manuel.miranda@idonial.com (M.M.-M.)

check for updates

**Abstract:** This study explores the potential antibiofouling capacity of coatings based on mixes of poly vinyl alcohol (PVA)-glutaraldehyde (GA) incorporating additions of metal and metal oxide nanoparticles ($TiO_2$, ZnO, CuO, AgNPs and Ag-$TiO_2$NPs). Such a kind of hybrid polymer-nanoparticle mix (PVA/GA/ nanoparticles (NPs)) was uniformly applied by spin coating on the surface of a laboratory raceway and tested in freshwater loaded with green algae communities. The results showed PVA/GA was a convenient carrier for the nanoparticles tested. Image analysis of the coatings showed that Ag-$TiO_2$ nanoparticles exhibited a significant improvement of the antibiofouling effect when compared with that of AgNPs and $TiO_2$-NPs. The effect of the Ag-$TiO_2$ NPs loaded coating about four times better than that of ZnO-NPs. A consistent experimental methodology was developed to test the antibiofouling capacity of the coatings and the hybrid coatings developed have demonstrated promising results as environmentally friendly antibiofouling materials.

**Keywords:** metal and metal oxide nanoparticles; Ag-$TiO_2$NPs; antibiofouling; poly (vinyl alcohol) (PVA); glutaraldehyde (GA); microalgae

## 1. Introduction

The accumulation on wet surfaces (natural or artificial) of undesirable microorganisms (bacteria, diatoms and spores of microalgae) is commonly known as fouling or biofouling [1]. Biofouling causes problems for microalgae farming in open culture systems (raceways) [2], due to pipes and valves clogging [3] and components corrosion. To prevent them it is vital to investigate and develop antibiofouling coatings of the surfaces in contact with the fluid.

Such active coatings, capable of preventing the adhesion of such microorganisms, could be based on the use of amphiphilic polymers [4] such as polyvinyl alcohol (PVA). PVA is a biodegradable polymer soluble in water, and available in different degrees of hydrolysis, with potential as an antibiofouling nanoparticles (NPs) carrier. Its low toxicity [5] ability to form thin films [6–10] and stabilize nanoparticles [11] are known. However, aqueous media can produce PVA swelling and dissolve it, consequently producing open structures and lowering the continuity of its coatings [12]. Therefore, it is necessary to balance the hydrophilic and hydrophobic properties by controlled cross-linking [13] using multifunctional compounds, such as dialdehydes [14], dicarboxylic acids [15] and dianhydrides [16]. Chemical crosslinking is a versatile method to improve mechanical, thermal and chemical stability of polymers [17]. Glutaraldehyde (GA) is an attractive PVA crosslinking agent,

since its reaction with the PVA's hydroxyl groups [18,19] is easily promoted by a mineral acid, such as HCl [20].

Metallic nanoparticles, such as copper [21] and silver, incorporated into polymeric matrices could be considered a new hybrid coating material given their potential advantages, but the latter must be proven. Copper shows an excellent antimicrobial activity against a wide range of microorganisms [22,23]. Silver nanoparticles (AgNPs) and silver-doped formulations are also interesting when working in biological environments, since they are considered safer and less toxic than other heavy metal-based formulations. In addition, the application of nano-silver on surfaces is known to be very versatile, allowing wide flexibility of use [24–26]. It has been demonstrated that the incorporation of metal oxide nanoparticles, such as ZnO, CuO and TiO$_2$ [27–29] in polymer matrices has improved the antibiofouling properties of some coatings. However, according to recent studies, the antibiofouling power of TiO$_2$ nanoparticles decreases markedly on substrates with a rough and porous surface. This surface morphology promotes the retention of water and nutrients, favoring the growth of biomass and reducing the oxides inhibitory effect [30,31].

In this work, the antibiofouling capacity of a thin film coat, based on PVA crosslinked with GA, doped with metal and metal oxides nanoparticles was applied by spin coating. Silver and metal oxide nanoparticles (ZnO, CuO and TiO$_2$) were synthesized by a seed and growth technique [32] and a sol–gel method [33] and added to the polymer matrix. The effect of the combined incorporation of nanosized Ag and TiO$_2$ was also studied.

The effect of these different coatings was investigated by immersing the coated substrates in a laboratory-scale raceway with a *Coelastrella* microalgae culture. The antibiofouling capacity of each coating was evaluated through image analysis after different immersion times (15 and 30 days) [34,35].

## 2. Materials and Methods

### 2.1. Chemicals and Materials

All chemicals used were of analytical grade. Polyvinyl alcohol (M.W. 500–5000, high purity, hydrolyzed) was obtained from Acros Organics. Silver nitrate (AgNO$_3$, >99% pure), zinc chloride, copper (II) chloride, sodium hydroxide, trisodium citrate dehydrate and glutaraldehyde (GA) were purchased from Merck Millipore. Tannic acid (TA), titanium tetraisopropoxide (TTIP), isopropanol, nitric acid (HNO$_3$), hydrochloric acid (HCl), sodium hydroxide (NaOH) and ethanol (EtOH) were obtained from VWR-Chemicals.

### 2.2. Synthesis of Nanoparticles (NPs)

Metal oxide nanoparticles were synthesized by a sol–gel route. Silver nanoparticles (AgNPs) were synthesized by a seed and growth method [32,33]. For both routes, the targeted size of the final nanoparticles was around 100 nm.

### 2.2.1. Synthesis of Titanium Dioxide Nanoparticles (TiO$_2$-NPs)

Briefly described, 5 mL TTIP solution were slowly dissolved in 15 mL of isopropanol and 250 mL of milli-Q water. The solution was refluxed at 60 °C for 6 h. Subsequently, 0.5 M HNO$_3$ was added dropwise, and a white precipitate was observed [36–40]. The precipitate obtained was isolated by filtration and washing with a mixture of hot water and organic solvents in order to remove adsorbed impurities. A thermal treatment was necessary to improve the crystallinity of amorphous compounds [41]. In our case, to obtain the greatest possible transformation into crystalline anatase, the resulting amorphous white solid was calcined at 450 °C for 10 h.

### 2.2.2. Synthesis of Zinc Oxide Nanoparticles (ZnO-NPs)

Solutions 0.4 M ZnCl$_2$ and 0.2 M NaOH were prepared in ethanol (EtOH) by ultrasonic dispersion of the solids during 5 min, followed by heating at 60 °C for 20 min. The required volumes of

the reactants were separately transferred to similar quantities of the solvent (25 mL) to obtain the desired concentrations of $ZnCl_2$ and NaOH in separate recipients. The solutions were mixed under, vigorous stirring at room temperature. The particles obtained were separated by sedimentation of the supernatant. The suspension was washed with distilled water to remove the NaCl residues that have formed. The particles were collected after the removal of EtOH by centrifugation (15 min at 6000 rpm). Washing and centrifugation were repeated 3 times. Finally, a thermal treatment of 5 h at 250 °C was carried out [42].

### 2.2.3. Synthesis of Copper Oxide Nanoparticle (CuO-NPs)

Until pH 14 was reached, 0.1 M NaOH was slowly dropped on a 0.1 M $CuCl_2$ solution under vigorous stirring. The black precipitate obtained was washed with deionized water and absolute ethanol for several times until neutral pH. Subsequently, the washed precipitates were dried at 80 °C for 16 h. Finally, they were calcined at 500 °C for 4 h [43].

### 2.2.4. Synthesis of Silver Nanoparticles (AgNPs)

AgNP colloidal suspensions with an average particle diameter of 100 nm were prepared according to the method described previously by Puntes et al. [32], through the reduction of silver nitrate by means of sodium citrate and tannic acid.

### 2.2.5. Synthesis of Ag-Doped Titanium Dioxide Nanoparticles (Ag-TiO$_2$NPs)

Ag-doped $TiO_2$ NPs were synthesized by a sol–gel procedure by using titanium isopropoxide (TTIP) and silver nitrate ($AgNO_3$) as precursors. A 0.1 M TTIP solution was prepared in absolute ethanol. Under stirring conditions, 5 wt %. $AgNO_3$ solution in distilled water was added. The mixture was kept still under stirring for 2 hours. The mixture was further dried at 100 °C for 48 h to obtain the Ag-$TiO_2$ gel. After aging during 24 h the Ag-$TiO_2$ gel was filtered and dried. Finally, the precipitates were calcined at 400–600 °C for 24 h [44,45].

### 2.3. Coating Procedure

Prior to surface coating, the substrates were immersed in ethanol, sonicated for 10 min, rinsed with deionized (DI) water three times and then dried at room temperature overnight.

PVA gel was prepared by completely dissolving 5 g of polymer powder in Milli-Q water, under magnetic stirring, at 60 °C, for about 30 min. The 5% (% by weight) PVA solution was allowed to cool to room temperature. To achieve the hydrogel, a [PVA]/[GA] mixture (% by weight) with a 4:1 ratio was prepared [46]. The mixture was vigorously stirred for 1 h at 70 °C and acidic pH was achieved by addition of 1 M HCl [20].

Preparation of nanoparticles doped PVA/GA coating was achieved through the addition of 5 wt % water suspension nanoparticles as described in Section 3.4.1.

In order to prepare a uniform thin film, spin coating was applied. This way, the coating solution was deposited on the flat substrates at a constant rate. The thickness of the film was determined by centrifugal forces controlled by spin speed, solution viscosity, and spin time [47]. The solution of PVA/GA/NPs was poured on the precleaned substrate spinning at 3000 rpm for 30 s (Figure 1). This process was repeated three times, in order to get a film of appropriate thickness. The coated specimen was then dried 24 h at room temperature.

A freshwater raceway ($110 \times 29.5 \times 28.0$ cm$^3$, containing 80 L water) equipped with a water circulation system was used throughout the study to test the antibiofouling capacity of the different coatings (Figure 2a). Coated specimens were placed on the walls of the raceway tank by using clothespins (Figure 2b). A *Coelastrella* microalgae culture (supplied by Neoalgae (Asturias, Spain)) was used as a model system (Figure 2c).
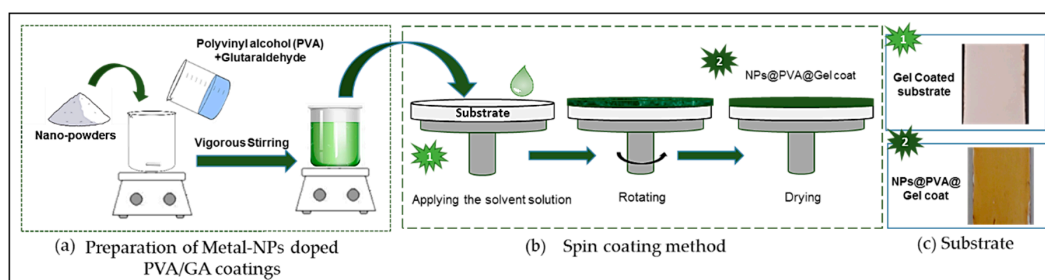
**Figure 1.** Schematic description of the coating method: (**a**) preparation of metal-nanoparticles (NPs) doped PVA/GA coatings; (**b**) NP deposition by spin coating and (**c**) example of the appearance of the coated substrate.
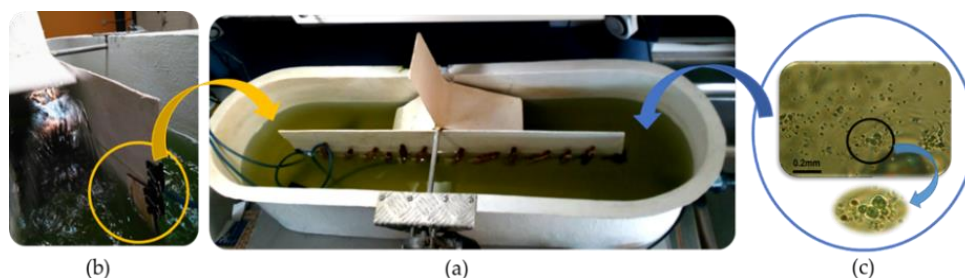


**Figure 2.** Summary of the laboratory raceway (**a**) freshwater raceway; (**b**) positioning of the substrates in the raceway and (**c**) optical microscopy of a culture of *Coelastrella* microalgae.

*2.4. Characterization Techniques*

Surface morphology of the synthetized nanoparticles was characterized with a field emission gun scanning electron microscope (GeminiSEM, ZEISS, Oberkochen, Germany) at an accelerating voltage of 20 kV. The HR-SEM was coupled with energy dispersive X-ray spectroscopy (EDX).

The crystal structure of the synthesized nanoparticles was studied using a D8 X-ray diffractometer (Bruker AXS GmbH, Karlsruhe, Germany) with filtered CuK$\alpha$ radiation. All samples were evaluated over the diffraction angles (2$\theta$) range of 20–80°.

The particle size analysis was carried out by dynamic light scattering (DLS). Powders were suspended (0.01 g/100 mL) in milli-Q water and sonicated for 30 s at 25°C °C.

The specimen's surfaces were characterized by Fourier Transform Infrared Spectroscopy (FTIR), before and after the coat application. Spectra—in the range of wavenumber from 400 to 4000 cm$^{-1}$ during 64 scans—were recorded on a Fourier-transform infrared spectrometer (Nicolet 6700, Thermo Scientific, Massachusetts, USA) using an ATR diamond crystal.

Once tested in the raceway, coated substrates were examined using an optical microscope (Olympus DP72, Tokyo, Japan) at 20× magnification, in order to assess the adhesion of microalgae. All coated surfaces were examined by digital image processing making use of Image-J software.

Surface roughness was characterized with a Perthometer (Perthometer, S 6 P, Mahr GmbH, Göttingen, Germany). The measurements were carried out by scanning the surface of the sample with a very sharp needle, in order to define its profile. For the roughness assessment, the specimen was divided in three sections.

## 3. Results and Discussion

*3.1. NPs Characterization*

The morphology of the as-prepared synthesized nanoparticles was observed by field emission gun scanning electron microscopy (FEG-SEM). The nanoparticles were spherical and relatively monodispersed. The diameter distribution ranged from 90 to 150 nm. The composition of the

nanoparticles was obtained by EDX analysis, confirming the absence of impurities. Furthermore, the crystalline nature of the synthesized nanoparticles was confirmed by XRD. All the results are collected in Figure A1 in Appendix A.

Hydrodynamic diameter of each particle in suspension was investigated by DLS. Table 1 summarizes the results. The polydispersity index (PDI) was used to estimate the average uniformity of the particle suspension. It is accepted that a sample is considered monodisperse when the PDI value is less than 0.1 [48]. As observed in Table 1, the PDI of all the synthesized particles were around 0.1, therefore they can be considered monodisperse. These results agree with the sizing found by the SEM observation.

**Table 1.** Summary of the size (hydrodynamic diameter) and polydispersity index (PDI) values obtained for the synthetized nanoparticles.

| Metal-NPs | Size (nm) | Polydispersity Index (PDI) |
|-----------|-----------|----------------------------|
| $TiO_2$ | 110.0 | 0.127 |
| ZnO | 112.9 | 0.100 |
| CuO | 104.2 | 0.101 |
| AgNPs | 100.9 | 0.152 |
| Ag-$TiO_2$ | 135.2 | 0.144 |

## 3.2. Substrate Characterization

The commercial materials used for the construction of raceway ponds are fiber reinforced polymers substrates and their surfaces are generally treated with different types of gel coatings. The raceway employed in this study was manufactured in fiber reinforced polyester by PROAGINOR S.A.L. (Asturias, Spain).

Rectangular specimens of gel coated substrates (dimensions $5.0 \times 2.5 \times 0.5$ cm$^3$; see Figure 3a) were surface treated by applying the different coatings developed in this study before being tested in order to evaluate their antibiofouling capacity.
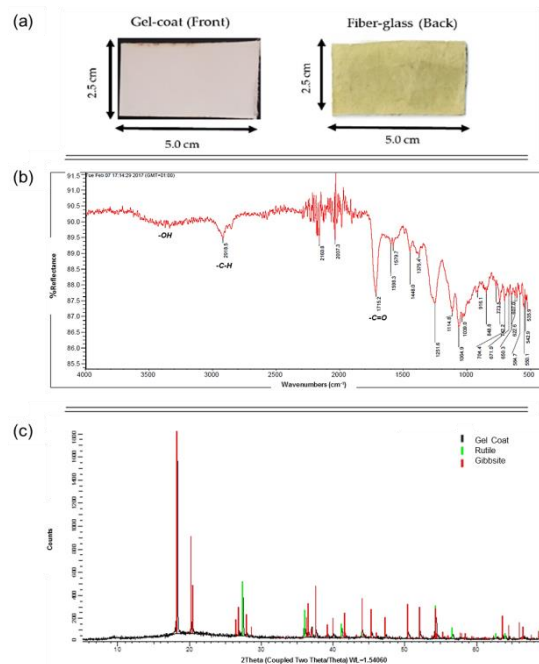


**Figure 3.** Substrate characterization: (**a**) front and back appearance of the original substrate; (**b**) FTIR characteristic spectrum for gel-coated surface and (**c**) XRD pattern of gel-coated surface.

The specimen's surfaces were characterized by Fourier transform infrared spectroscopy (FTIR). Figure 3b shows the characteristic bands of alcohol group at 3500 cm$^{-1}$, probably from the hardeners or curatives co-reactants. A band around 1750 cm$^{-1}$ attributed to the - C = O groups is also observed. Bands in the range of a wavenumber from 1500 to 400 cm$^{-1}$ were difficult to assign, but that information is complementary to that given by the X-ray diffraction patterns of the specimen substrate. Figure 3c shows the presence of rutile (TiO$_2$) and gibbsite (Al (OH)$_3$) as main phases.

The surface roughness can affect the hydrodynamic performance of antibiofouling coatings and the settlement of microalgae. Therefore, it was considered an important parameter in the evaluation of the novel coatings [49]. Surface roughness measurements were carried out on three substrate specimens, and three different sections of each one, as explained in Section 2.4. The arithmetic mean roughness (Ra) was taken as the representative parameter of the roughness of the substrate surface. The average roughness obtained for the three substrate specimens was 0.46 µm (see Table 2). This low value for initial roughness of the gel-coat face should favor the uniformity of the subsequently applied coating.

**Table 2.** Results of the roughness test of our substrate.

| Gel-Coat (Surface) | Cutoff Length (cm) | Roughness (Ra) Average (µm) | Total Roughness (Ra) Average (µm) | Standard Deviation |
|---|---|---|---|---|
| | 1.65 | 0.42 | | |
| Substrate 1 | 3.30 | 0.41 | 0.42 | 0.015 |
| | 4.95 | 0.44 | | |
| | 1.65 | 0.46 | | |
| Substrate 2 | 3.30 | 0.48 | 0.46 | 0.025 |
| | 4.95 | 0.43 | | |
| | 1.65 | 0.57 | | |
| Substrate 3 | 3.30 | 0.40 | 0.49 | 0.085 |
| | 4.95 | 0.50 | | |
| Mean value | | | 0.46 | |

### 3.3. PVA/GA Conditioning and Characterization

In order to obtain a coating as uniform as possible, the experimental conditions and formulations were optimized. For the hydrogel preparation, a PVA/GA mixture (% by weight) with a 4:1 ratio was found as suitable according to the literature [46]. A semiquantitative analysis of the FTIR spectra of PVA and PVA cross-linked with GA was carried to monitor the chemically cross-linking between PVA and GA and characterize the products. The FTIR spectra shown in Figure 4 (FTIR spectra of PVA/GA (Figure 4b)) reveal two important bands at 2850 and 2750 cm$^{-1}$ of C-H stretching related to aldehydes, an absorption duplet with peaks attributed to the alkyl chain [19]. Additionally, a strong band from carbonyl group was verified (C = O at 1720–1740 cm$^{-1}$). These bands overlapped with PVA bands in these regions. However, by crosslinking PVA with GA, the O–H stretching vibration peak at 3330–3350 cm$^{-1}$ was relatively decreased when compared to pure PVA. This could indicate a possible formation of acetal bridges. Moreover, the C-O stretching at approximately 1100 cm$^{-1}$ in pure PVA was replaced by a broader absorption band (from 1000 to 1140 cm$^{-1}$), which can be attributed to the ether (C-O) and the acetal ring (C-O-C). According to the literature, these acetal bridges could be considered as confirmation of the PVA/GA crosslinking reaction [50].
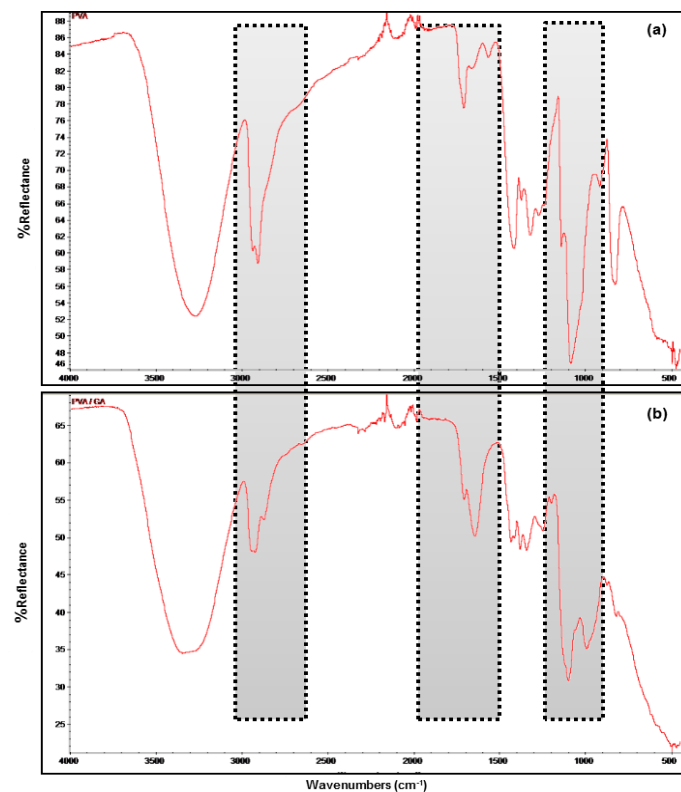
**Figure 4.** FTIR spectra from: (**a**) pure PVA and (**b**) PVA crosslinked by glutaraldehyde (GA).

## 3.4. Substrate Coating

### 3.4.1. Preparation of Metal-NPs Doped PVA/GA Coatings

To produce our antifouling coating, an ex situ method was used. This means that the particles were synthesized before their incorporation into the polymer, the matrix being just the dispersion medium: 5 wt % suspensions of nanoparticles were prepared in distilled water and sonicated for 1 h. Then, aliquots were added to the previously prepared hydrogel PVA/GA as described in Section 2.3. The mixture was stirred for 10–15 min and later on its was kept under ultrasounds for approximately 2 h to obtain a uniform suspension [51].

### 3.4.2. Coating Characterization

Two and three-dimensional surface images of the modified substrate membranes are displayed in Figure 5, where bright and dark areas correspond to the peak and valleys, respectively. The surface roughness parameters measured for the surface coating are listed in Table 3. Measurements were carried out following the same protocol as those for the uncoated substrate. The arithmetic mean roughness (Ra) was taken as the most representative parameter of the roughness of the surface.

Figure 5 confirms that the different dissolutions were uniformly extended by spin coating on the substrate surface.

The results obtained, by digital image processing (Figure. 5), and the roughness quantitative data (Table 3), show: (i) the unmodified PVA/GA coating (Figure 5a) to have an average roughness of 0.95 μm, which is close to the roughness obtained for the as received substrate, which was 0.46 μm, demonstrating the uniformity of the coating; (ii) a uniform distribution of peak-to-valley morphology can be observed for the coatings of PVA/GA/TiO$_2$-NPs, PVA/GA/Ag-NPs and PVA/GA/Ag-TiO$_2$-NPs, average roughness of 2.1, 5.0 and 1.46 μm respectively; (iii) PVA/GA/ZnO-NPs coating showed the roughest surface. Its average roughness value, obtained as an average of three coated specimens was

9.8 µm, closely followed by PVA/GA/CuO-NPs coating, average roughness 9.28 µm. These data will be taken into account in the discussion of the antibiofouling coating effect.
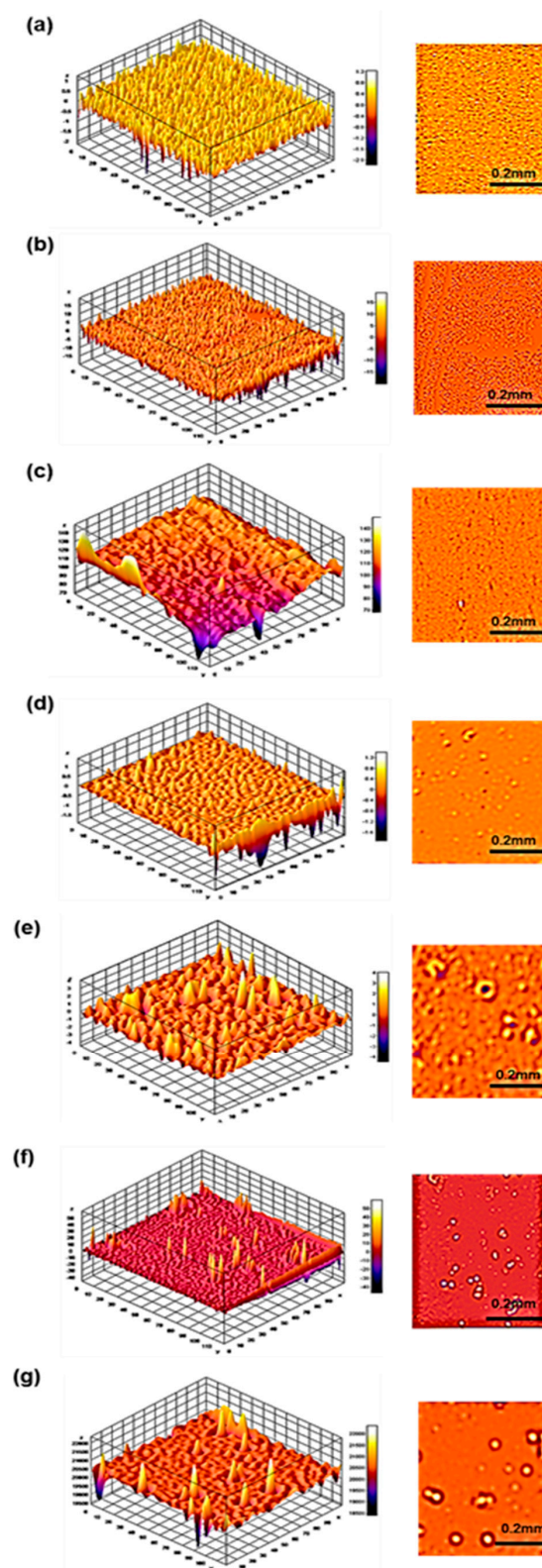


**Figure 5.** Three- and two-dimensional images of all coating studied: (**a**) original substrate; (**b**) PVA/GA coating; (**c**) PVA/GA/AgNPs; (**d**) PVA/GA/TiO$_2$-NPs; (**e**) PVA/GA/ZnONPs; (**f**) PVA/GA/Ag-TiO$_2$NPs and (**g**) PVA/GA/CuONPs.

**Table 3.** Roughness test results for the different coatings applied to the substrate.

| Coating Surface | Cutoff Length (cm) | Roughness (Ra) [1] Average (µm) | Total Roughness (Ra) Average (µm) | Standard Deviation |
|---|---|---|---|---|
| PVA/GA | 1.65 | 0,89 | | |
| | 3.30 | 0,95 | 0.95 | 0.06 |
| | 4.95 | 1,02 | | |
| PVA/GA/AgNPs | 1.65 | 4.90 | | |
| | 3.30 | 5.12 | 5.0 | 0.2 |
| | 4.95 | 4.94 | | |
| PVA/GA/TiO$_2$-NPs | 1.65 | 2.00 | | |
| | 3.30 | 2.31 | 2.1 | 0.2 |
| | 4.95 | 1.98 | | |
| PVA/GA/ZnO-NPs | 1.65 | 9.74 | | |
| | 3.30 | 9.91 | 9.8 | 0.1 |
| | 4.95 | 9.68 | | |
| PVA/GA/Ag-TiO$_2$-NPs | 1.65 | 1.43 | | |
| | 3.30 | 1.52 | 1.46 | 0.06 |
| | 4.95 | 1.41 | | |
| PVA/GA/CuO-NPs | 1.65 | 9.22 | | |
| | 3.30 | 9.35 | 9.28 | 0.07 |
| | 4.95 | 9.26 | | |

[1] Roughness average is the result of the measurements that were carried out on three substrate specimens.

### 3.5. Evaluation of the Antifouling Behaviour of NPs Doped Coatings Against Green Algae in Freshwater

The surface of the commercial substrate coated only with PVA/GA (Figure 6) was taken as reference for the evaluation of all NP containing coatings. After fifteen and thirty days immersion in the culture tank, the surface was visually inspected. Once the samples had been immersed for fifteen days, green accretions could already be observed covering the surface of the control substrate. After another fifteen days (one month of immersion), the green algae accretions had continued growing and formed a dense layer over the whole exposed surface.
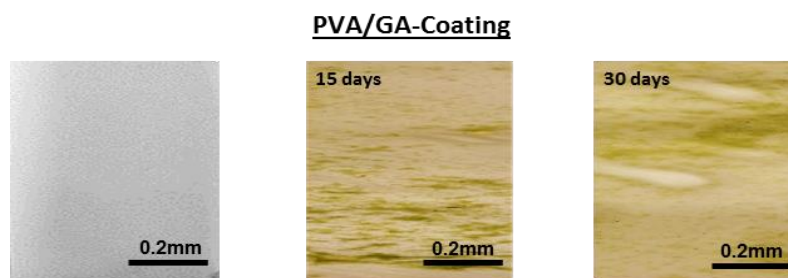
**PVA/GA-Coating**



**Figure 6.** Qualitative antifouling test image of the PVA/GA coating surfaces observed at immersion times of 15 days and 30 days.

In any case after 30 days of immersion the coating remained stable, an indication of the high reliability of the PVA/GA coat when immersed in fresh water.

In order to check the long-term stability and antifouling capacity of the MP modified-coatings, their surfaces were also visually inspected after fifteen days and one-month immersion in the *Coelastrella* microalgae culture in freshwater.

To prove the inhibitory effect on microalgae adhesion, images of the different NP coatings were taken by optical microscopy. In addition, the signal intensity of the captured images was digitized using Image-J 1.53t-win-java8 software for all specimens tested. Optical density results are shown in Figure 7. Each value obtained is the mean of the measurements in each specimen (*n* = 3), and the error bar corresponds to the standard deviation. The low values for the standard deviation confirm the reproducibility of the measurements.
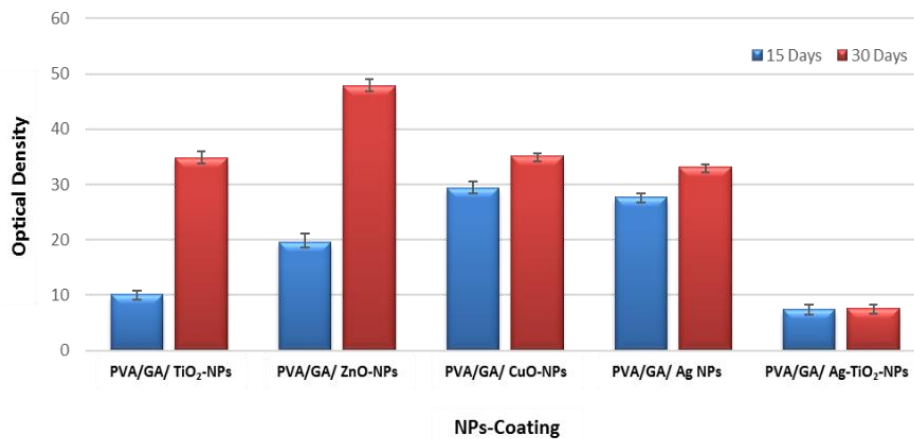
**Figure 7.** Optical density analysis of the metallic nanoparticle coatings at immersion times of 15 days (blue) and 30 days (red). The error bars indicate the standard deviation of 3 measurements.

In order to observe biofouling on the NP modified coated surfaces and be able to carry out an optical density (OD) analysis, the color contrast on the images was modified. Figure 8 shows the images obtained by optical microscopy after 15 days and 30 days of immersion times.



**Figure 8.** Qualitative antifouling assessment by optical microscopy of: (**a**) PVAGA, (**b**) PVAGA/TiO2-NPs, (**c**) PVAGA/ ZnO-NPs, (**d**) PVAGA/CuO-NPs, (**e**) PVAGA/AgNPs and (**f**) PVAGA/Ag-TiO2-NPs coatings, after 15 days and 30 days.

Figure 8 shows that under the same conditions, coatings based on CuO-NPs (Figure 8d) and Ag NPs (Figure 8e), hardly underwent any changes in their surface between 15 and 30 days of the immersion, keeping the microalga layer deposited on the coating practically constant.

For TiO$_2$ NPs doped coating (Figure 8b), increased adhesion of microalgae was observed in relation to immersion time. Three times more deposition was recorded between its inspection at day 15 and that after one-month immersion.

Ag-TiO$_2$NPs doped coatings (Figure 8f), in turn, did not present changes in relation to immersion time. This NP treatment showed the highest antibiofouling capacity among those investigated in this work.

In the case of the ZnO-NPs coating (Figure 8c), the deposition of microalgae observed after one month was twice the value of the optical density (OD) at day 15, and two times higher that of the TiO$_2$-NPs coating after both periods. If compared with the Ag-TiO$_2$-NPs coating, fouling with the ZnO-NPs coating was up to four times higher. Based on the current literature this effect could be related to the nanosize. Jones et al. [52] describe the relationship between the nanoparticles size and the nano-ZnO toxicity. They indicated that 5-nm particles had a five-fold stronger toxic effect than 50–70-nm particles. Then, the standard size selected in this work (close to 100 nm) is likely to decrease the effectiveness of the NPs. On the other hand, a certain nanomaterial aggregation is perhaps acting as a limitation for ion release mechanism due to the loss of surface area. Finally, these effects for the nano-ZnO depend also on the environmental conditions of the test [53].

As already mentioned, the roughness of the NP doped coating could play an important role, because it favors the growth of the microalgae and the accumulation of nutrients. The ZnO-NPs doped coating had an average roughness of 9.8 μm. This value could be considered very high as compared to the Ag-TiO$_2$NPs doped coatings, the most efficient ones, which were characterized with the lowest roughness values (1.46 μm, Table 3). These results confirm that high roughness is not desirable for antibiofouling capacity [30,31]. However, in the case of CuNPs incorporated into polymer nanocomposites, it has been shown that the antibiofouling capacity could be improved by increasing the load of CuNPs [54]. This could explain the fact that the CuO-NP-loaded coatings in this work were more effective than ZnO-NPs loaded ones of similar roughness (9.28 and 9.8 respectively).

The comparison of all NP loaded coatings here studied (Figures 7 and 8) indicates that the coating based on PVA/GA/Ag-TiO$_2$NPs had the highest antifouling capacity against green *Coelastrella* microalgae in freshwater, in contrast with the coating based on ZnO-NPs, which showed the worst antifouling capacity under the same conditions.

In order to confirm that the nanoparticles are still present on the coating after the antifouling experiments, X-ray diffraction (XRD) analyses of PVA/GA/Ag-TiO$_2$-NPs and PVA/GA/ZnO-NPs coatings were carried out. Figure 9 shows both X-ray diffraction patterns (2θ range from 5° to 70°), which confirm the permanence of the nanoparticles.

The X-ray diffraction patterns show the presence of the PVA (in blue) in both cases. Figure 9a shows in red the characteristic pattern of anatase in the PVA/GA/Ag-TiO$_2$-NPs coating. AgNPs (in green) could not be detected due to the low crystallinity of the sample and the PVA used as a matrix in the coating. Figure 9b shows in red the pattern of ZnO in the PVA/GA/ZnO-NPs coating. These results confirm the viability of the hybrid materials investigated.
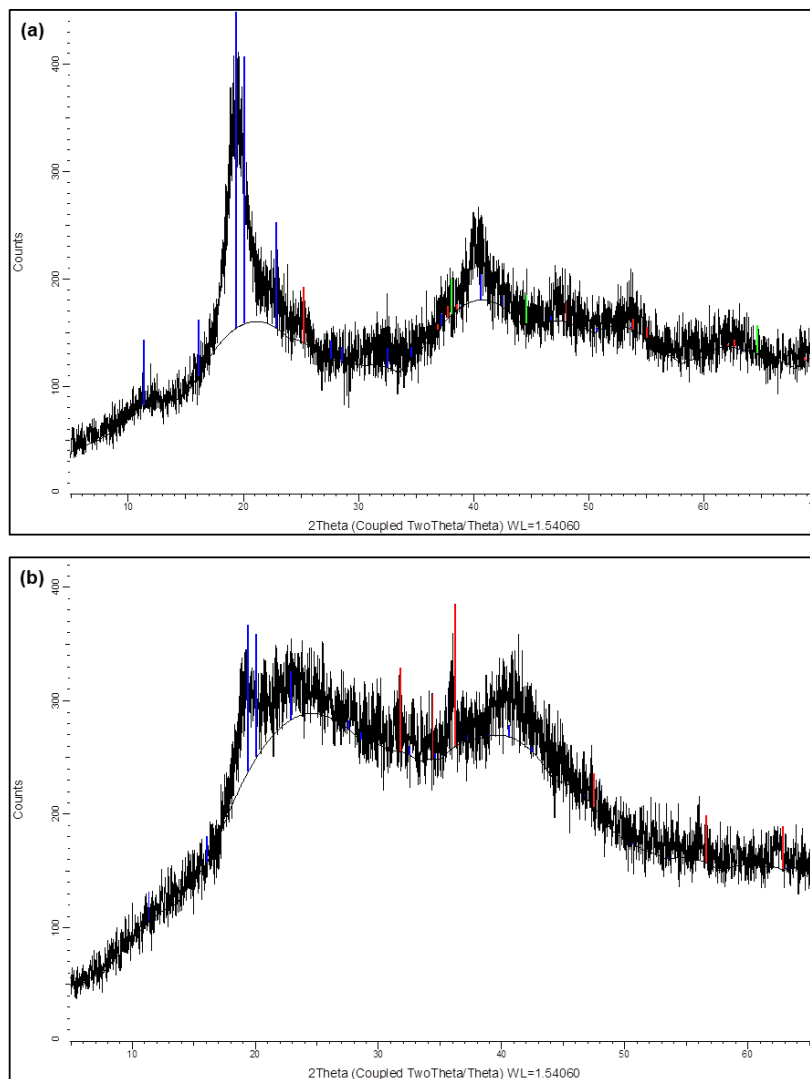
**Figure 9.** X-ray diffraction patterns from: (**a**) PVA/GA/Ag-TiO$_2$-NPs and (**b**) PVA/GA/ZnO-NPs.

## 4. Conclusions

Stable coats of PVA/GA doped with different metal oxide and metal nanoparticles (NPs), referred to as hybrid polymer-nanoparticle mixes, were successfully produced and applied by spin coating onto a commercial gel coated fiber reinforced polyester substrate.

The antibiofouling capacity of such NP doped coatings was studied at a laboratory-scale in a raceway filled with a *Coelastrella* microalgae culture, and a consistent experimental methodology was developed to test the antibiofouling capacity of such coatings.

Image analysis, specifically optical density, was used to evaluate the antifouling behavior, and capacity, of each NPs doped coat system.

NP doping of the system PVA-GA proved to be a realistic and viable alternative to coat the commercial substrates used in the construction of raceways for culture of microalgae.

For the NP hybrid systems studied no influence was observed on the viability of the microalgae culture itself.

The coating based on PVA/GA/ZnO nanoparticles was the one with the least antibiofouling capacity: approximately four times more fouling appeared on the surface than that of a surface cover by the PVA/GA/ Ag-TiO$_2$ NP system.

Finally, the PVA/GA/Ag-TiO$_2$NPs coating showed the highest antifouling capacity against green *Coelastrella* microalgae in freshwater.

It remains to be further investigated whether these results are ultimately related to each nanoparticle size, or even the roughness of each of the coatings.

## Appendix A. Structural and Morphological Characterization of the Nanoparticles Synthesized

Structural and morphological characterizations of the nanoparticles were performed by: energy dispersive X-ray spectroscopy (EDX), field emission gun scanning electron microscopy (FEG-SEM) and X-ray diffraction (XRD).

Figure A1 shows the result obtained for the characterization by EDX, SEM and XRD of: (a) $TiO_2$-NPs, (b) ZnO-NPs, (c) CuO-NPs, (d) AgNPs and (e) Ag-$TiO_2$-NPs.
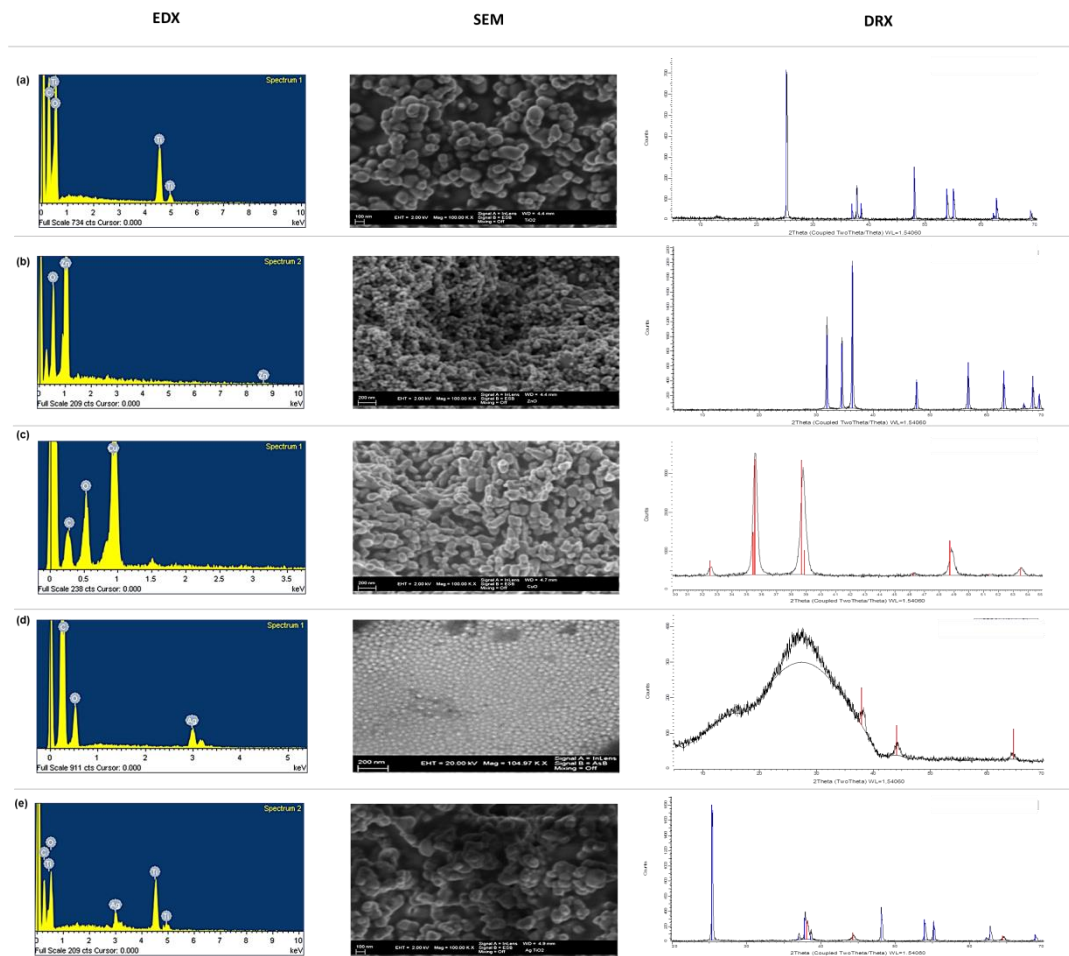


**Figure A1.** NPs characterization by EDX, SEM and XRD of: (**a**) $TiO_2$-NPs, (**b**) ZnO-NPs, (**c**) CuO-NPs, (**d**) AgNPs and (**e**) Ag-$TiO_2$-NPs.

## References

1. Margaillan, A.; Bressy, C. Fouling release coatings: A nontoxic alternative to biocidal antifouling coatings. *Chem. Rev.* **2012**, *112*, 4347–4390.
2. Posten, C. Design principles of photo-bioreactors for cultivation of microalgae. *Eng. Life Sci.* **2009**, *9*, 165–177. [CrossRef]
3. Ren, J.; Han, P.; Wei, H.; Jia, L. Fouling-resistant behavior of silver nanoparticle-modi fi ed surfaces against the bioadhesion of microalgae. *ACS Appl. Mater. Interfaces* **2014**, *6*, 3829–3838. [CrossRef] [PubMed]
4. Kamoun, E.A.; Kenawy, E.R.S.; Chen, X. A review on polymeric hydrogel membranes for wound dressing applications: PVA-based hydrogel dressings. *J. Adv. Res.* **2017**, *8*, 217–233. [CrossRef] [PubMed]
5. Saharudin, K.A.; Sreekantan, S.; Basiron, N.; Khor, Y.L.; Harun, N.H.; Rabiatul, R.B.; Akil, H.M.; Seeni, A.; Vignesh, K. Bacteriostatic activity of LLDPE nanocomposite embedded with sol-gel synthesized TiO2/ZnO coupled oxides at various ratios. *Polymers (Basel)* **2018**, *10*, 878. [CrossRef]
6. Cha, W.; Hyon, S.; Ikada, Y. Transparent poly (viny alcohol) hydrogel with high water content and high strength. *Makromol. Chern* **1992**, *1925*, 1913–1925. [CrossRef]
7. Chem, C.T.; Chang, Y.J.; Chen, C.; Tobolsky, A. V formalized poly (viny alcohol) membranes for reverse osmosis. *J. Appl. Polym. Sci.* **1973**, *17*, 789–796. [CrossRef]
8. Hirai, T.; Asada, Y.; Suzuki, T.; Hayashi, S. Studies on elastic hydrogel membrane. I. Effect of preparation conditions on the membrane performance. *J. Appl. Polym. Sci.* **1989**, *38*, 491–502. [CrossRef]
9. Ibrahim, N.A. Preparation and characterization of carboxylic cation exchange resins from the reaction of poly (viny alcohol) with melamine-formaldehyde and some hydroxy acids. *Die Angew. Makromol. Chem.* **1993**, *210*, 7–20. [CrossRef]
10. Yamaura, K.; Itoh, M.; Tanigami, T. Properties of gels obtained by freezing/thawing of poly (vinyl alcohol)/water/dimethyl sulf oxide solutions. *J. Appl. Polym. Sci.* **1989**, *5*, 2709–2718. [CrossRef]
11. Kumar, R.; Siril, P.F. Preparation and characterization of polyvinyl alcohol stabilized griseofulvin nanoparticles. *Mater. Today Proc.* **2016**, *3*, 2261–2267. [CrossRef]
12. Katz, M.G.; Wydeven, T. Heat-treated membranes. *J. Appl. Polym. Sci.* **1982**, *27*, 79–87. [CrossRef]
13. Huang, R.Y.M.; Moreira, A.; Notarfonzo, R. Pervaporation separation of acetic acid-water mixtures using modified membranes. I. Blended polyacrylic acid (PAA). *J. Appl. Polym. Sci.* **1988**, *35*, 1191–1200. [CrossRef]
14. Gebben, B.; van den Berg, H.W.A.; Bargeman, D.; Smolders, C.A. Intramolecular crosslinking of poly(vinyl alcohol). *Polymer (Guildf)* **1985**, *26*, 1737–1740. [CrossRef]
15. Kormeyer, R.W.; Peppas, N.A. Effect of morphology of hydrophilic polimeric matrices on the diffusion and release of water soluble drugs. *J. Membr. Sci.* **1981**, *9*, 211–227. [CrossRef]
16. Gimenez, V.; Mantecon, A.; Cadiz, V. Crosslinking of poly(viny1 alcohol) using dianhydrides as hardeners. *J. Appl. Polym. Sci.* **1996**, *59*, 425–431. [CrossRef]
17. Marin, E.; Rojas, J. Preparation and characterization of crosslinked a films alcohol with waterprof properties. *Int. J. Pharm. Pharm. Sci.* **2015**, *7*, 242–248.
18. Figueiredo, K.C.S.; Alves, T.L.M.; Borges, C.P. Poly (vinyl alcohol) films crosslinked by glutaraldehyde under mild conditions. *J. Appl. Polym. Sci.* **2008**, *111*, 3074–3080. [CrossRef]
19. Mansur, H.S.; Sadahira, C.M.; Souza, A.N.; Mansur, A.A.P. FTIR spectroscopy characterization of poly (vinyl alcohol) hydrogel with different hydrolysis degree and chemically crosslinked with glutaraldehyde. *Mater. Sci. Eng. C* **2008**, *28*, 539–548. [CrossRef]
20. Khan, M.Q.; Kharaghani, D.; Ullah, S.; Waqas, M.; Abbasi, A.M.R.; Saito, Y.; Zhu, C.; Kim, I.S. Self-cleaning properties of electrospun PVA/TiO2 and PVA/ZnO nanofibers composites. *Nanomaterials* **2018**, *8*, 644. [CrossRef]
21. Graziani, L.; Quagliarini, E.; Orazio, M.D. The role of roughness and porosity on the self-cleaning and anti-biofouling efficiency of TiO 2 -Cu and TiO 2 -Ag nanocoatings applied on fired bricks. *Constr. Build. Mater.* **2016**, *129*, 116–124. [CrossRef]
22. Grass, G.; Rensing, C.; Solioz, M. Metallic copper as an antimicrobial surface. *Appl. Environ. Microbiol.* **2011**, *77*, 1541–1547. [CrossRef] [PubMed]
23. Medina, C.; Santos-Martinez, M.J.; Radomski, A.; Corrigan, O.I.; Radomski, M.W. Nanoparticles: Pharmacological and toxicological significance. *Br. J. Pharmacol.* **2007**, *150*, 552–558. [CrossRef] [PubMed]

24. Zhang, Y.; Wan, Y.; Shi, Y.; Pan, G.; Yan, H.; Xu, J.; Guo, M.; Qin, L.; Liu, Y. Facile modification of thin-film composite nanofiltration membrane with silver nanoparticles for anti-biofouling. *J. Polym. Res.* **2016**, *23*, 1–9. [CrossRef]

25. Loo, C.Y.; Young, P.M.; Lee, W.H.; Cavaliere, R.; Whitchurch, C.B.; Rohanizadeh, R. Non-cytotoxic silver nanoparticle-polyvinyl alcohol hydrogels with anti-biofilm activity: Designed as coatings for endotracheal tube materials. *Biofouling* **2014**, *30*, 773–788. [CrossRef] [PubMed]

26. Rajaeian, B.; Heitz, A.; Tade, M.O.; Liu, S. Improved separation and antifouling performance of PVA thin film nanocomposite membranes incorporated with carboxylated TiO2 nanoparticles. *J. Membr. Sci.* **2015**, *485*, 48–59. [CrossRef]

27. Balta, S.; Sotto, A.; Luis, P.; Benea, L.; Bruggen, B.; Kim, J. A new outlook on membrane enhancement with nanoparticles: The alternative of ZnO. *J. Memb. Sci.* **2012**, *389*, 155–161. [CrossRef]

28. Sawada, I.; Fachrul, R.; Ito, T.; Ohmukai, Y.; Maruyama, T.; Matsuyama, H. Development of a hydrophilic polymer membrane containing silver nanoparticles with both organic antifouling and antibacterial properties. *J. Memb. Sci.* **2012**, *387–388*, 1–6. [CrossRef]

29. Pourjafar, S.; Rahimpour, A.; Jahanshahi, M. Synthesis and characterization of PVA/PES thin film composite nanofiltration membrane modified with TiO 2 nanoparticles for better performance and surface properties. *J. Ind. Eng. Chem.* **2012**, *18*, 1398–1405. [CrossRef]

30. Hou, X.; Huang, M.; Wu, X.; Liu, A. Preparation and studies of photocatalytic silver-loaded TiO 2 films by hybrid sol—gel method. *Chem. Eng. J.* **2009**, *146*, 42–48. [CrossRef]

31. Sá, J.; Agüera, C.A.; Gross, S.; Anderson, J.A. Applied catalysis B: Environmental photocatalytic nitrate reduction over metal modified TiO 2. *Appl. Catal. B Environ.* **2009**, *85*, 192–200. [CrossRef]

32. Bastús, N.; Merkoçi, F.; Piella, J.; Puntes, V. Synthesis of highly monodisperse citrate- stabilized silver nanoparticles of up to 200 nm: kinetic control and catalytic properties. *Chem. Mater.* **2014**, *26*, 2836–2846. [CrossRef]

33. Pierre, A.C.; Bernard-lyon, U.C. Porous sol-gel ceramics. *Ceram. Int.* **1997**, *23*, 229–238. [CrossRef]

34. Bartley, G.E.; Scolnik, P.A. Plant carotenoids: Pigments for photoprotection, visual attraction, and human health. *Plant Cell* **1995**, *7*, 1027–1038. [PubMed]

35. Abd EI Baky, H.H.; EI-Baroty, G.S. Healthy Benefit of microalgal bioactive substances. *J. Aquat. Sci.* **2013**, *1*, 11–23.

36. Chen, X.; Mao, S.S. Titanium dioxide nanomaterials: Synthesis, properties, modifications, and applications. *Chem. Rev.* **2007**, *107*, 2891–2959. [CrossRef]

37. Guzmán-Velderrain, V.; López, Y.O.; Gutiérrez, J.S.; De Investigación, C.; De Nanotecnología, L.N.; De Materiales, D. TiO 2 films synthesis over polypropylene by Sol-Gel Assisted with hydrothermal treatment for the photocatalytic propane degradation. *Green Sustain. Chem.* **2014**, *4*, 120–132. [CrossRef]

38. Mahshid, S.; Askari, M.; Ghamsari, M.S. Synthesis of TiO2 nanoparticles by hydrolysis and peptization of titanium isopropoxide solution. *J. Mater. Process. Technol.* **2007**, *189*, 296–300. [CrossRef]

39. Hussain, M.; Ceccarelli, R.; Marchisio, D.L.; Fino, D.; Russo, N.; Geobaldo, F. Synthesis, characterization, and photocatalytic application of novel TiO2 nanoparticles. *Chem. Eng. J.* **2010**, *157*, 45–51. [CrossRef]

40. Nyamukamba, P.; Okoh, O.; Mungondori, H.; Taziwa, R.; Zinya, S. Synthetic methods for titanium dioxide nanoparticles: A review. *InterchOpen* **2018**, *8*, 151–175.

41. Ovenstone, J.; Yanagisawa, K. Effect of hydrothermal treatment of amorphous Titania on the Phase change from anatase to rutile during calcination. *Chem. Mater.* **1999**, *32*, 2770–2774. [CrossRef]

42. Vega-Poot, A.G.; Rodrıguez-Gattorno, G.; Soberanis-Domnguez, O.E.; Patiño-Dıaz, R.T.; Espinosa-Pesqueira, M.; Oskam, G. The nucleation kinetics of ZnO nanoparticles from ZnCl 2 in ethanol solutions. *Nanoscale* **2010**, *2*, 2710–2717. [CrossRef] [PubMed]

43. Phiwdang, K.; Suphankij, S.; Mekprasart, W. Synthesis of CuO nanoparticles by precipitation method using different precursors. *Energy Procedia* **2013**, *34*, 740–745. [CrossRef]

44. Ahamed, M.; Khan, M.A.M.; Akhtar, M.J.; Alhadlaq, H.A. Ag-doping regulates the cytotoxicity of TiO2 nanoparticles via oxidative stress in human cancer cells. *Sci. Rep.* **2017**, *7*, 1–14.

45. Durango-Giraldo, G.; Cardona, A.; Zapata, J.F.; Santa, J.F.; Buitrago-Sierra, R. Titanium dioxide modified with silver by two methods for bactericidal applications. *Heliyon* **2019**, *5*, e01608. [CrossRef]

46. Mansur, H.S.; Mansur, A.A.P. Small angle X-Ray scattering, FTIR and SEM characterization of nanostructured PVA/TEOS hybrids by chemical crosslinking. *Mater. Res. Soc. Symp. Proc.* **2005**, *873*, 1–6. [CrossRef]

47. Ranganayaki, T.; Venkatachalam, M.; Vasuki, T.; Shankar, S. Preparation and characterization of nanocrystalline TiO2 thin films prepared by Sol-Gel spin coating method. *Int. J. Innov. Res. Sci. Eng. Technol.* **2014**, *3*, 16708–16711.

48. Clayton, K.N.; Salameh, J.W.; Wereley, S.T.; Kinzer-Ursem, T.L. Physical characterization of nanoparticle size and surface modification using particle scattering diffusometry. *Biomicrofluidics* **2016**, *10*, 054107. [CrossRef]

49. Howell, D.; Behrends, B. A review of surface roughness in antifouling coatings illustrating the importance of cutoff length. *Biofouling* **2006**, *22*, 401–410. [CrossRef]

50. dos Reis, E.F.; Campos, F.S.; Lage, A.P.; Leite, R.C.; Heneine, L.G.; Vasconcelos, W.L.; Lobato, Z.I.P.; Mansur, H.S. Synthesis and characterization of poly (vinyl alcohol) hydrogels and hybrids for rMPB70 protein adsorption. *Mater. Res.* **2006**, *9*, 185–191. [CrossRef]

51. Sugumaran, S.; Bellan, C.S. Transparent nano composite PVA–TiO2 and PMMA–TiO2 thin films: Optical and dielectric properties. *Opt. Int. J. Light Electron Opt.* **2014**, *125*, 5128–5133. [CrossRef]

52. Jones, N.; Ray, B.; Ranjit, K.T.; Manna, A.C. Antibacterial activity of ZnO nanoparticle suspensions on a broad spectrum of microorganisms. *FEMS Microbiol. Lett.* **2008**, *279*, 71–76. [CrossRef]

53. Li, M.; Zhu, L.; Lin, D. Toxicity of ZnO nanoparticles to escherichia Coli: Mechanism and the influence of medium components. *Environ. Sci. Technol.* **2011**, *45*, 1977–1983. [CrossRef] [PubMed]

54. Cioffi, N.; Torsi, L.; Ditaranto, N.; Tantillo, G.; Ghibelli, L.; Sabbatini, L.; Bleve-Zacheo, T.; D'Alessio, M.; Zambonin, P.G.; Traversa, E. Copper nanoparticle/polymer composites with antifungal and bacteriostatic properties. *Chem. Mater.* **2005**, *17*, 5255–5262. [CrossRef]